

MICROSTRUCTURAL EVOLUTION AND MECHANICAL CHARACTERIZATIONS OF AL-TiC MATRIX COMPOSITES PRODUCED VIA FRICTION STIR

KARAKTERIZACIJA ALUMINIJA IN TITANA KARBIDA KOVINSKIH MATRICA KOMPOZITOV JIH PROIZVAJA TRENJE MEŠATI VARJENJE

Abegunde O. Olayinka, Akinlabi T. Esther, Madyira M. Daniel

Department of Mechanical Engineering Science, Faculty of Engineering and Built Environment, University of Johannesburg, Auckland Park Kingsway Campus, Johannesburg, South Africa. 2006

oabegunde@uj.ac.za

ABSTRACT

In this research work, ample study was conducted on the material characterization of aluminium (Al) and titanium carbide (TiC) metal matrix composites produced via friction stir welding. Different process parameters were employed for the welding process. Rotational speeds of 1600 rpm to 2000 rpm at an interval of 200 rpm and traverse speeds of 100 to 300 mm/min at an interval of 100 mm/min were employed for the welding conducted on an Intelligent Stir Welding for Industry and Research (I-STIR) Process Development System (PDS) platform. The characterizations carried out include optical microscopy and the scanning electron microscopy analyses combined with Energy Dispersive Spectroscopy (SEM/EDS) techniques to investigate the particle distribution, microstructural evolution and the chemical analysis of the welded samples. Vickers microhardness tests were used to determine the hardness distribution of the welded zone and tensile testing was conducted to quantify the strength of the welded area to the base metal in order to establish the optimal process parameters. Based on the results obtained from the characterization analysis, it was found that the process parameters played a major role in the microstructural evolution. Homogenous distribution of the TiC particles was observed at high rotational speed of 2000 rpm and low traverse speed of 100 mm/min. The highest hardness value was measured at the stir zone of the weld due to the presence of the TiC reinforcement particles. The tensile strength also increased as the rotational speed increased and 92% joint efficiency was recorded in a sample produced at 2000 rpm and 100 mm/min. The EDS analysis revealed that Al, Ti and C made up the composition formed at the stir zone. The optimum process parameter setting was found to be at 2000 rpm and 100 mm/min and can be recommended.

Keywords: friction stir welding, metal matrix composite, aluminium, titanium carbide, mechanical properties, microstructural evolution

V tem raziskovalnem delu, je obsežna študija o materialni karakterizaciji aluminija (Al) in titanovega karbida (TiC) kovinskih kompozitov, proizvedene s pomočjo trenja mešalne varjenja. Različne procesne parametre smo uporabili za varilnega procesa. Rotacijski hitrosti 1600 rpm do 2000 rpm v razmaku 200 vrtljaji na minuto in prečnih hitrostjo 100 do 300 mm / min pri razmiku 100 mm / min je bilo zaposlenih za varjenje na inteligentne Primesamo varjenjem za industrijo in raziskave (I-Stir) Razvoj Process sistem (PDS) platformo. Za karakterizacijo izvajajo vključuje optično mikroskopijo in vrstično elektronsko mikroskopijo analize v kombinaciji z energijo disperzijsko spektroskopijo (SEM / EDS), tehnike za preiskavo porazdelitve delcev, mikrostrukture razvoj in kemijsko analizo varjenih vzorcih. Vickers testi mikrotrdote je bila uporabljena za določitev trdote porazdelitev zvarnega coni in natezno testiranje je bilo izvedeno količinsko moč zvarnega vrata z osnovno kovino, da bi ugotovili optimalnih procesnih parametrov. Na osnovi rezultatov, dobljenih z analizo opredeljuje, je bilo ugotovljeno, da so procesni parametri igral pomembno vlogo v mikrostrukturne evolucije. Homogena porazdelitev TiC delcev opazili pri visokih hitrostih vrtenja 2000 obratov na minuto in nizke prečno hitrostjo 100 mm / min. Največja vrednost trdote smo izmerili pri mešalne cone zvara zaradi prisotnosti ojačitvenih delcev TiC. Natezna trdnost povečala tudi poveča hitrost vrtenja in 92% skupne učinkovitosti je bila najdena v vzorcu proizvedeno pri 2000 obratih na minuto in 100 mm / min. Analiza je pokazala, da EDS Al, Ti in C sestavljena sestavka tvorjen na mešalne cone. Optimalni proces parameter je bilo ugotovljeno, da je pri 2000 obratih na minuto in 100 mm / min in se lahko priporočljivo.

Ključne besede: trenje stir varjenje , metal matrix kompozitni , aluminij , titan karbida , mehanske lastnosti , mikrostruktura

1 INTRODUCTION

Metal matrix composites (MMCs) reinforced with ceramic phases exhibit high stiffness, high elastic modulus, improved resistance to wear, creep and fatigue, which make them promising structural materials for aerospace and automobile industries over monolithic metals. However, these composites also suffer from a significant loss in ductility and toughness due to the incorporation of non-deformable ceramic reinforcements, which limits their applications especially where ductility of the material is a determinant factor in materials selection¹. Aluminium metal matrix (AMC) is a variant of MMCs which has potential of replacing many conventional engineering

materials. AMCs have already found commercial applications in the defence, aerospace, automobile and marine industries due to their favourable metallurgical and mechanical properties ²⁻⁵. The metal matrix is Aluminium and the reinforcement can be any ceramic particles compatible with the metal matrix.

In recent years, several techniques have been reported for manufacturing AMCs. Plasma air spraying, stir casting, squeeze casting, molten metal infiltration and powder metallurgy were reported for producing bulk composites while high energy laser melt injection, plasma spraying, cast sinter and electron beam irradiation have been used for producing surface AMCs ^{6,7}. Nevertheless, it should be pointed out that most of these existing processing techniques for forming composites are generally based on liquid phase processing at high temperatures. In this case, it is hard to avoid the interfacial reaction between reinforcement and the metal matrix and the formation of some detrimental phases ¹.

Friction stir welding FSW is a solid state welding process developed by TWI for welding aluminium and its alloys ⁸. It has been used to successfully weld aluminium alloys ⁹⁻¹¹ and also used to weld other metals like magnesium, copper and titanium ¹²⁻¹⁴. FSW is another emerging potential technique that can be employed for producing AMCs. Since the process is a solid state welding process, it is envisaged to alleviate the problems associated with interfacial reaction, melting of ceramics and formation of detrimental phases during manufacturing of AMCs.

Research studies have been reported on friction stir processing of Aluminium matrix composites ¹⁵⁻¹⁸. These studies concluded that grain refinement was achieved using FSW process. Improved particle distribution and higher mechanical properties were also observed. Also reported is that the process parameters used for welding and the tool geometry played major role in the outcome result. Based on the available literature, previous research works have been limited to surface composite using FS process for modification of the surface properties.

In this study, AMCs were produced using FSW and Titanium carbide TiC was used as the reinforcement particles. The addition of the TiC ceramic particles is due to its favourable mechanical properties which include high melting point, better fracture and tribological resistance. The preference of FSW process for production of Al-TiC composite is to avoid delamination (a failure when laminated material becomes separated, perhaps induced by poor processing during production, impact in service, or some other means which lead to separations of layers of reinforcement), debonding (when two materials stop adhering to each other), incompatible mixing of base materials and filler materials, presence of porosity, inhomogeneous distribution, (clustering), segregation of grain at boundaries, wetting of the particles, excess eutectic formation, melting of ceramic particles and formation of undesirable deleterious phase usually experienced in other techniques. FSW is also advantageous due to rapid removal of reaction products from interface which enhances further reaction

The effect of process parameters on the weld microstructure, microhardness and tensile behaviour was studied and the optimal process parameters were established.

2 EXPERIMENT

2.1 Preparation, dimensions and composition of workpieces

Aluminium 1050 alloy sheets of 300 mm × 200 mm × 3 mm with smooth surface finishing were used for this research work. These materials were manufactured and supplied by Metal Tool and Trade, South Africa. The chemical composition of the aluminium as per manufacturer Material Safety Data Sheet (MSDS) is shown in Table 1.

Before the welding process, V-grooves with depth of 1.5 mm and width of 3 mm were made on all the aluminium sheets using a milling machine and the titanium carbide particles were filled and compacted into the grooves as illustrated schematically in Figure 1.

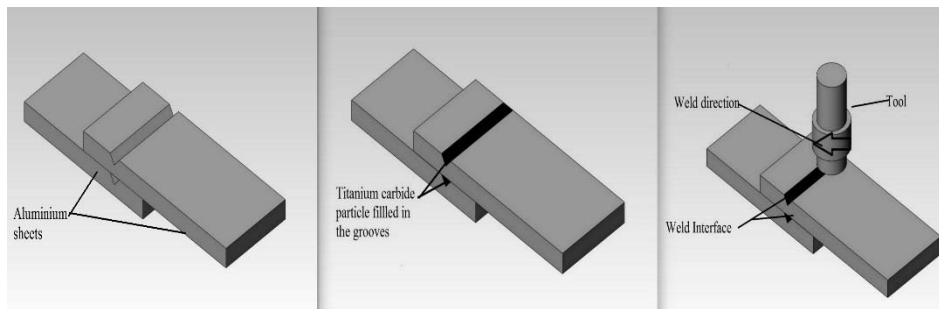


Figure 1 Schematic illustration of FSW of Al/TiC process

Slika 1 : Shematski prikaz FSW Al / TiC procesa

2.2 FSW tool

The FSW tool used is a cylindrical H13 steel tool hardened to 52 HRC shown in Figure 2



Figure 2 FSW Tool

Slika 2 FSW

A basic tool geometry was used with a tool length of 5.7 mm and tool diameter of 6 mm. The tool shoulder diameter is thrice the pin diameter (18 mm) and concave in geometry to exert pressure on the workpiece during welding.

2.3 Friction stir welding platform

The experimental setup of the samples properly positioned and firmly clamped on the backing plate is shown in Figure 3. The welding was performed on an Intelligent Stir Welding for Industry and Research (I-STIR) Process Development System (PDS) at the eNtsa of Nelson Mandela Metropolitan University, Port Elizabeth, South Africa. Table 1 summarizes the different welding parameters used to produce the welds. Tilt angle of 3° was kept constant and used for all the different welding parameters.



Figure 3 Experimental weld setup of FSW platform

Slika 3 Eksperimentalni zvar postavitev FSW platforme

Table 1 FSW process parameters

Tabela 1 FSW procesnih parametrov

| Weld number | Rotational speed (rpm) | Traverse speed (mm/min) | Weld Interface | Weld pitch (mm/rpm) |
|-------------|------------------------|-------------------------|----------------|---------------------|
| A1 | 1600 | 100 | With TiC | 0.063 |
| A2 | 1600 | 200 | With TiC | 0.125 |
| A3 | 1600 | 300 | With TiC | 0.188 |
| B1 | 1800 | 100 | With TiC | 0.056 |
| B2 | 1800 | 200 | With TiC | 0.111 |
| B3 | 1800 | 300 | With TiC | 0.167 |

| | | | | |
|----|------|-----|-------------|-------|
| C1 | 2000 | 100 | With TiC | 0.050 |
| C2 | 2000 | 200 | With TiC | 0.100 |
| C3 | 2000 | 300 | With TiC | 0.150 |
| D1 | 1600 | 200 | Without TiC | 0.125 |
| D2 | 1800 | 200 | Without TiC | 0.111 |
| D3 | 2000 | 200 | Without TiC | 0.100 |

A backing plate was positioned between the bed of the FSW platform and the workpiece. The choice of the backing plate is for proper dissipation of heat during the welding process. A supporting sheet of the same thickness was placed underneath the upper plate to help align and stabilize the sheets to be joined during welding.

2.4 Samples preparation and testing

Before sectioning the samples for various characterization with a water jet cutting machine, the flashes created during welding were removed from the weld seams. The metallographic samples preparation was done in accordance to ASTM E3-95 for microstructure analysis¹⁹. The samples were sectioned perpendicular to the weld direction. Grinding and polishing were carefully done on the samples to obtain mirror finished samples. Keller's reagent was used for etching for proper observation of the grains. DP25 Olympus optical microscope and scanning electron microscope with energy dispersive spectrometry (SEM + EDS) were used for the microstructural analysis. To evaluate the mechanical properties, Vickers microhardness and Instron tensile testing were used. The Vickers hardness was done in accordance with ASTM E92-82E3 standard²⁰. Load of 100 g and dwell time of 10 seconds were used. The tensile tests were carried out using a load cell capacity of 100 kN at crosshead rate of 1 mm/min. No fewer than three lap tests were done for each process parameter. Since there is no test standard for friction stir lap joints, ASTM E8/E8M-13a and ASTM D1002^{21, 22} for shear strength of single lap joint adhesively bonded metal specimen (tension loading of metal-to-metal) were used as the reference test standard for lap shear test. Fractography was performed on the fractured surface of the tensile samples to determine the mode of failure.

3 RESULTS AND DISCUSSION

3.1 Weld surface visual observation

The top surfaces of the welded samples under different welding process parameters are shown in Figure 4. The visual assessment of the weld surfaces show no typical physical defects like wormhole, cracks and void.

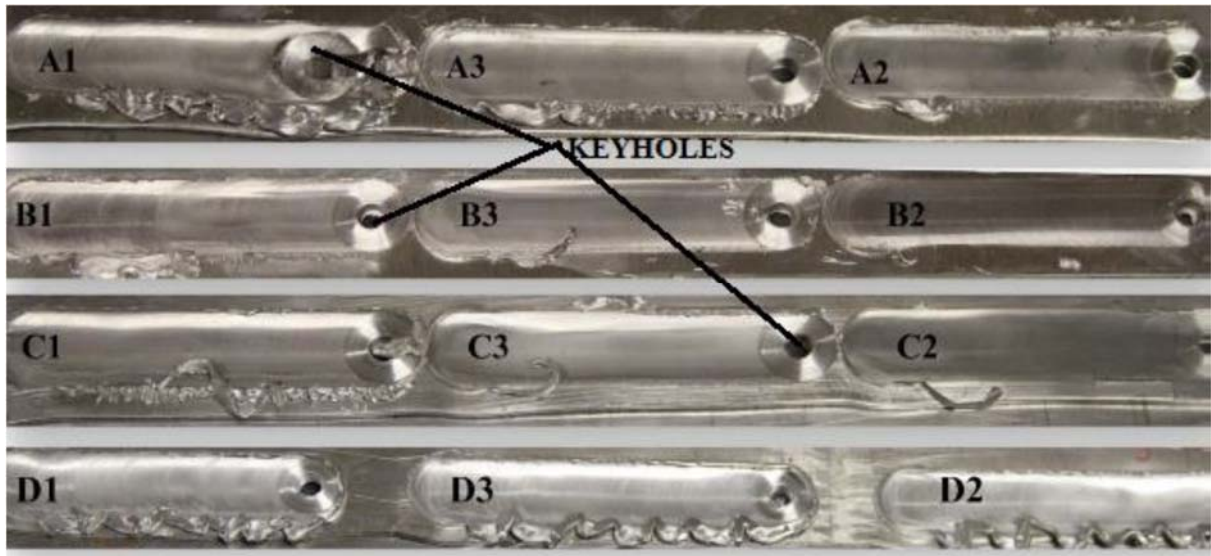


Figure 4 Top view of the processed FSW welds

Slika 4 Tloris predelanih FSW zvarov

The shape of the weld seam is slightly convex in nature, which is caused by the design of the tool shoulder. Semi-circular ripples effect caused by the action of the tool shoulder was also observed. This effect is referred to as wake effect. Keyholes were seen at the end of the weld seam. The depth of these keyholes shows the extent of penetration of the pin from the top to the bottom sheet. Flashes were observed for all the process parameters used and more on the welds produced without reinforcement particles. Most of the flashes were located on the retreating side of the weld due to the movement of the materials from the advancing side of the weld to the retreating side.






3.2 Microstructural evolution





Macrostructure

Table 2 summarizes the macrostructure pictures at cross section of the weld zone under different process parameters

Table 2 Macrostructure features at different process parameters

Tabela 2 makrostrukturne funkcije na različnih procesnih parametrah

| Weld number | Macrostructure | Nugget shape |
|-------------|---|--------------|
| A1 |  | Elliptical |
| A2 |  | Basin |
| A3 |  | Basin |
| B1 |  | Elliptical |
| B2 |  | Elliptical |

| | | |
|----|--|------------|
| B3 |  | Basin |
| C1 |  | Elliptical |
| C2 |  | Basin |
| C3 |  | Basin |

From Table 2, it can be seen that the process parameters have significant effect on the orientation of the FSW macrostructure. As the traverse speed increased from 100 mm/min to 300 mm/min using the same tool geometry, the geometry of the nugget zone changed from elliptical shape to basin-like shape. It is important to note that the formation of the basin shape is due to the effect of thermal heat transfer from the shoulder of the tool to the sheets. At high traverse speed of 300 mm/min, the heat generated is lower and most of the heat built up at the top sheet with minimal proportion of the heat sink into the bottom sheet. This makes the top sheet to undergo more thermal cycle by direct contact with the tool shoulder and severe plastic deformation than the bottom sheet causing the basin like shape to form. The intense plastic deformation and high temperature exposure experienced at the lower traverse speed resulted into the elliptical shape.

TiC Powder

The micrograph under SEM of the TiC powder used as the reinforcement in this research study is illustrated in Figure 5.

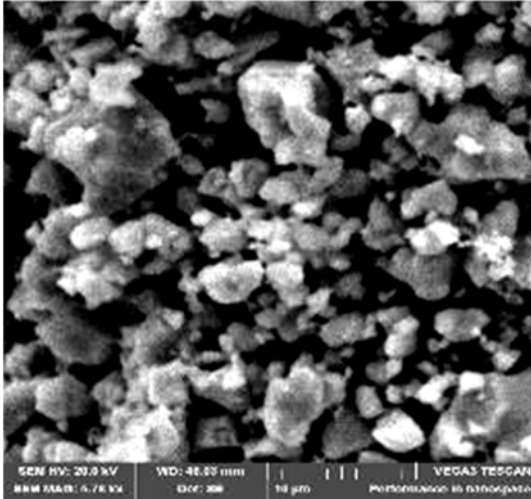


Figure 5 SEM Photomicrograph of TiC Powder

The morphology of the TiC powder is irregular shaped ball milled powder and grain size of about 2 microns

Microstructure

The pictorial overview of the microstructural evolution across different zones after FSW is presented in Figure 6. All the four zones, namely base metal (BM) close to the heat affected zone (HAZ), HAZ that is sandwiched by the BM and thermo-mechanically affected zone (TMAZ), TMAZ found on both sides of the stir zone (SZ) and the SZ were exhibited in the micrograph taken from the processed zones. The base metal retains its original microstructural features. The TMAZ and HAZ were formed on both the retreating and advancing sides of the welds. The grain structure in the HAZ shows elongated grain growth slightly different from the base material. The temperature experienced in the HAZ was enough to thermally activate grain growth but not sufficient enough to plastically deform the grain. In TMAZ, severely deformed grains are found, which are induced by drastic plastic deformation of SZ during FSW. In the SZ, the microstructure is characterized by dynamically recrystallized fine equiaxed grains owing to the drastic deformation induced by the sufficient stirring during welding of the top and bottom sheet. The distribution of the TiC reinforcement particles is a salient feature observed between the top and the bottom sheets around the SZ. At the top SZ, the presence of TiC is negligible and scanty but significant distribution was found at the bottom of the sheet. This indicates that during the welding process, the reinforcement particles experienced both downward and horizontal flow around the stir zone. Grains in the upper SZ are coarser than those in the bottom SZ. The heat during the FSW process mainly originates from the tool shoulder friction with the surface of the top sheet. Additionally, the heat in the bottom SZ can easily transfer into the bottom sheet and the backing plate. Therefore, the heat cycle of the bottom SZ is relatively lower. The grains in the upper SZ have more time to grow due to the higher temperature gradient.

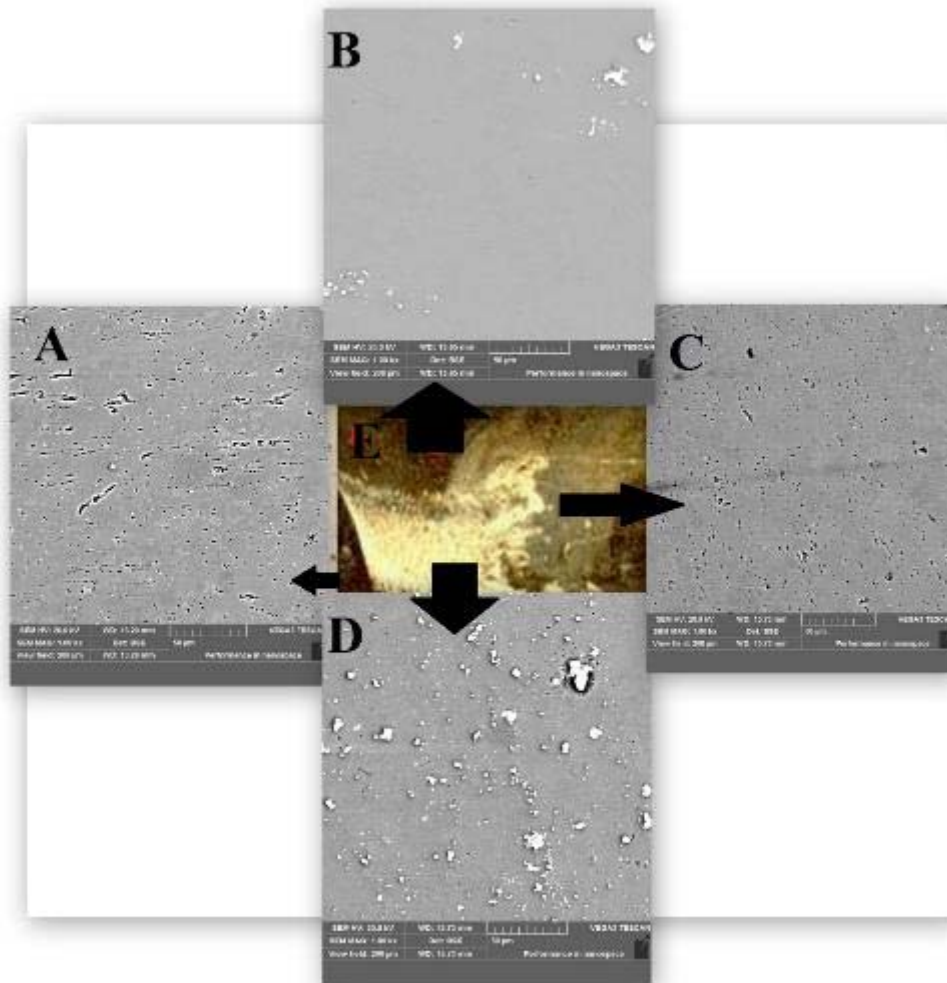


Figure 6 Microstructural evolution at different zones A) Thermo-mechanical affected zone, B) Upper stir zone, C) Heat affected zone, D) Lower stir zone E) Macrostructure of the weld zone at 2000 rpm and 300 mm/min

Slika 6 Mikrostrukturalna Napredek pri različnih conah A) termo - mehansko prizadeti coni B) Zgornji mešalna cona C) toplote prizadeti coni, D) spodnji mešalna cona E) makrostruktura varilnega področja pri 2000 obratih na minuto in 300 mm / min

Another notable observation from the microstructure is the transition region on the advancing side and the retreating side which is illustrated in Figure 7. On the advancing side (AS), the transition region is sharper and well defined and on the retreating side (RS), the transition region diffuse into the parent material. On the AS, the plastic deformation direction of the processed zone and the BM are in opposite direction, which resulted in

enormous relative deformation and the homogenous distribution of the TiC particles between the BM and the processed zone at the AS but the BM distorted and diffused smoothly together with the processed zone at the RS resulting in clustering of the reinforcement.

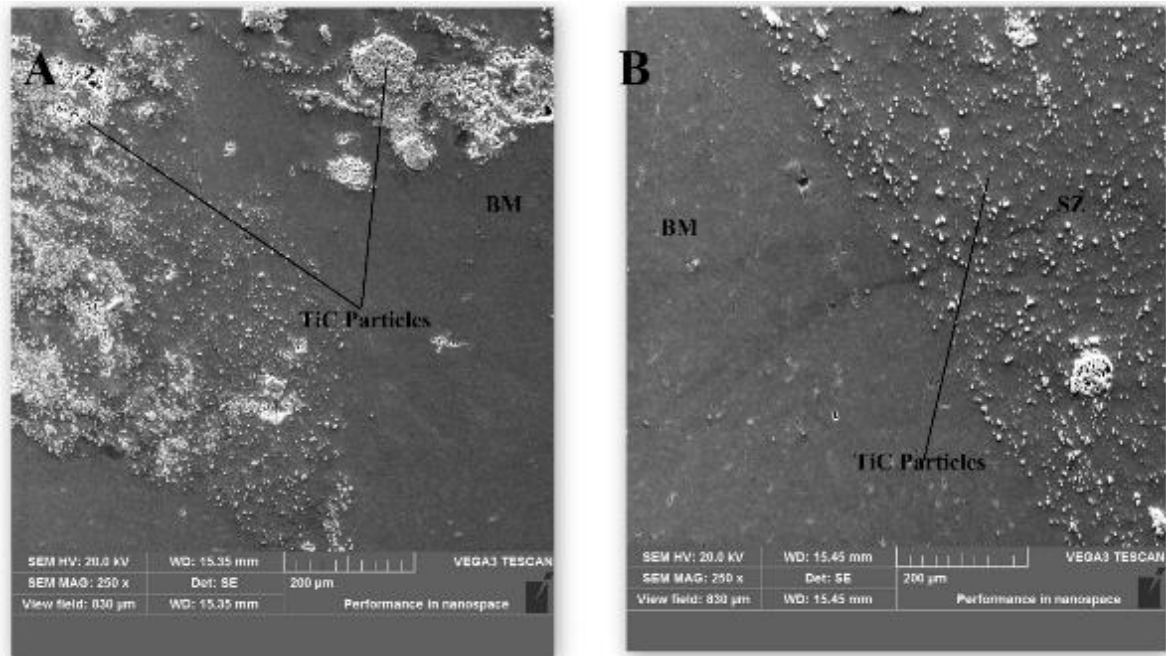


Figure 7 Transition zone A) Retreating side and B) Advancing side

Slika 7 Prehod cona A) Odcepljanje strani in B) Pospeševanje stran

It can be observed that the TiC reinforcement within the processed zone had undergone intense mixing and stirring resulting in breakup of the coarse TiC morphology. As the rotational speed of the weld increased from 1600 rpm to 2000 rpm, the distribution of TiC becomes more homogenous as shown in Figure 8. At rotational speed of 1600 rpm, the particles clustered together around the bottom sheet and at 2000 rpm, the particles were uniformly distributed around the stir zone.

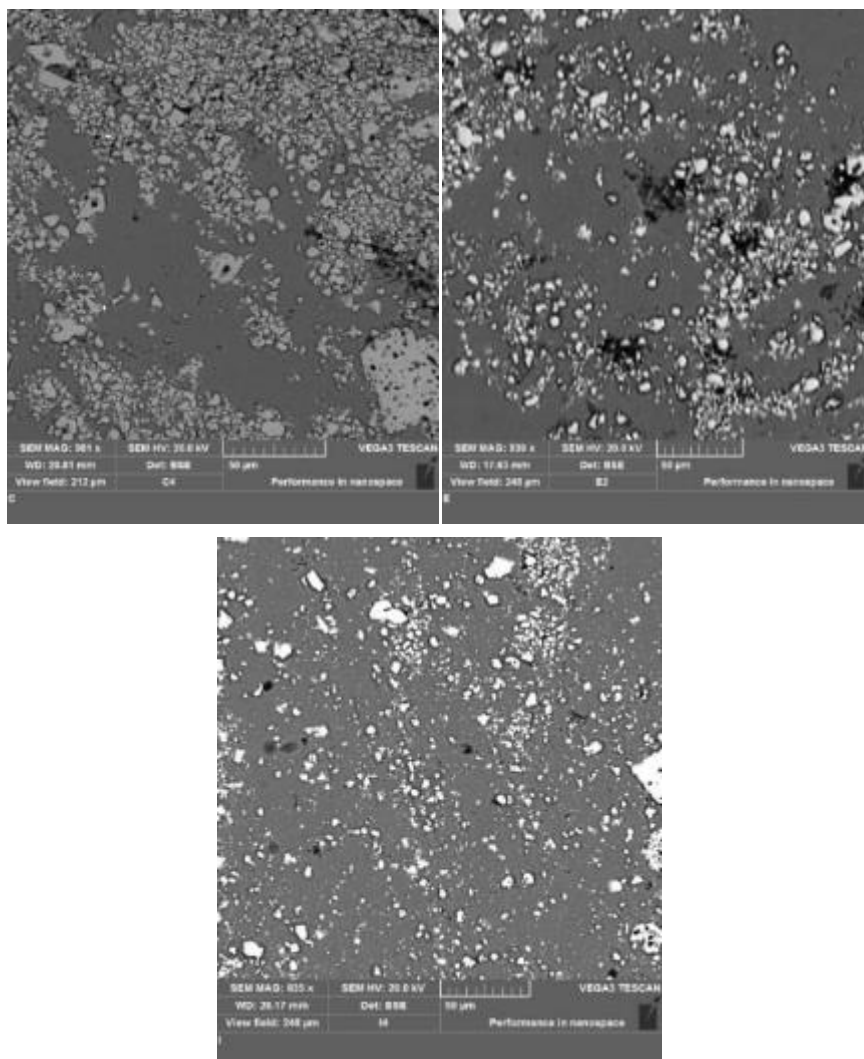


Figure 8 SEM Micrograph at traverse speed of 100 mm/min and rotational speed of A) 1600 rpm B) 1800 rpm and C) 2000 rpm

Slika 8 SEM mikrografija pri prečni hitrosti 100 mm / min in hitrost rotacije A) 1600 rpm B) 1800 vrtljaji na minuto in C) 2000 rpm

The contribution of intense deformation and high temperature exposure within the stir zone resulted into fragmentation, recrystallization and the development of refined texture within and around the stir zone at rotational speed of 2000 rpm. In addition, increase in traverse speed caused the particles to agglomerate in the stir zone. As traverse speed decreased, the grain size also decreased in the composite but increased in the pure aluminium samples without the reinforcement. This might be due to high heat input associated with low traverse

speed. The phenomenal effect of particle reinforcement on grain size refinement of the matrix is reported as *pinning effect*. According to pinning effect, the grain refinement by reinforcement particles increases with the decrease in the particle size and increase in volume fraction of the particles. Adequate heat input and stirring are responsible for deformation and recrystallization of the matrix with the reinforcement. At higher rotational speed of 2000 rpm and traverse speed of 100 mm/min, more uniform distribution of the TiC particles was found.

Energy Dispersive Spectroscopy Results

EDS analysis was performed on all the welds with reinforcement. The uniformly distributed particles were confirmed to be titanium and carbon as shown in Figure 9 which is the scan of the weld interface of the sample produced at rotational speed 2000 rpm and traverse speed 100 mm/min.

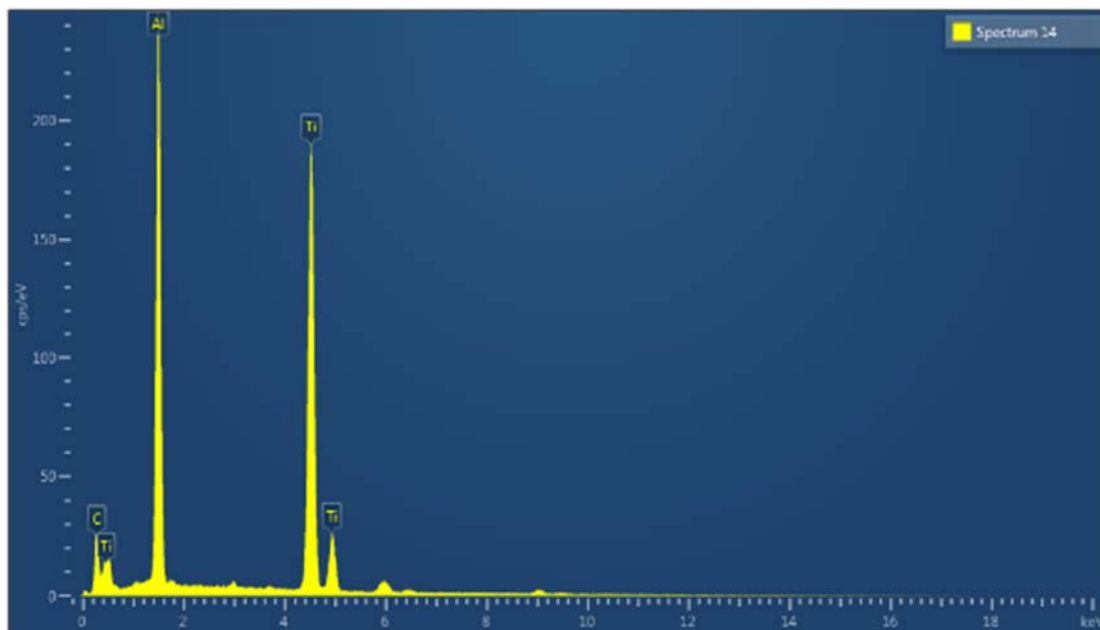


Figure 9 EDS from the weld interface at rotational speed of 2000 rpm and traverse speed of 100 mm/min

Slika 9 EDS iz vmesnika zvara pri vrtilni hitrosti 2000 obratov na minuto in prečni hitrosti 100 mm / min

The elemental composition by atomic weight at the stir zone is confirmed to be 72.04% of aluminium, 23.71% of carbon and 4.34% of titanium.

3.3 Microhardness Profiling

The Vickers hardness distribution is illustrated in Figure 10. The shape of the hardness distribution is a "W-sinusoidal". The lowest hardness value was found at the HAZ and the highest hardness value at the SZ. The

hardness value of the SZ increased by 58% when compared to the base metal for sample C1. Thangarasu ¹⁷ suggested four methods of hardening in FSW MMC namely:

- Orowan strengthening.
- Grain and substructure strengthening.
- Quench hardening resulting from the dislocations generated to accommodate the differential thermal contraction between the reinforcing particles and the matrix.
- Work hardening due to the strain misfit between the elastic reinforcing particles and the plastic matrix.

The increment in the hardness value at the SZ is attributed to grain refinement and the presence of reinforcement particles. Fragmentation of bigger TiC particles gave rise to dislocation density and dynamics recrystallization during welding, thereby producing finer grain size in the stir zone. These factors are responsible for higher hardness value in the stir zone of welds with the reinforcement particles. The minimum hardness value appeared at the HAZ. This is due to the thermal history experienced at this zone which resulted in the coarsening of the precipitates.

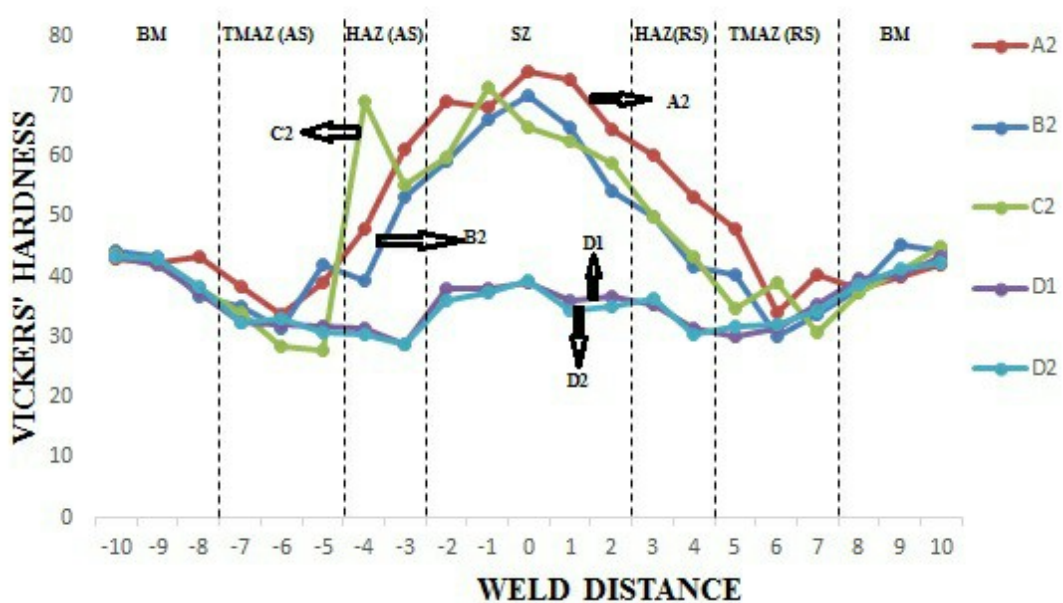


Figure 10 Hardness Profile of the FSL welds

Slika 10 Trdota Profil od FSL zvarov

Because of the distribution and the deposition of the TiC particles around the AS of the welded zone, AS size shows higher hardness value than the RS due to the fact that materials on the RS has lower time to rotate since the current flow of material is directly proportional to the time of flow on this side.

3.4 Tensile behaviour

In order to quantify the mechanical resistance of the FSWed joints, the ratio between the maximum transferred load by the specimens in shear test to the width of the specimen itself was considered. In this way, the values are shown for all the considered case. The average results of the three replica samples carried out are reported. Every sample was tested to failure. The shear fracture load per unit width of the FSWed of Al with and without the TiC composite at different process parameters are presented in Table 3

Table 3 Shear strength and joint efficiency of different welds

Tabela 3 Strižna trdnost in skupno učinkovitost različnih zvarov

| Weld number | Rotational speed (rpm) | Traverse speed (mm/min) | Weld Pitch (mm/rpm) | Average Shear Fracture Load per unit width (N/mm) | Joint efficiency % |
|-------------|------------------------|-------------------------|---------------------|---|--------------------|
| A1 | 1600 | 100 | 0.063 | 159 | 79.4 |
| A2 | 1600 | 200 | 0.125 | 150 | 60.8 |
| A3 | 1600 | 300 | 0.188 | 132 | 52.97 |
| B1 | 1800 | 100 | 0.056 | 185 | 90.51 |
| B2 | 1800 | 200 | 0.111 | 178 | 77.53 |
| B3 | 1800 | 300 | 0.167 | 170 | 68.60 |
| C1 | 2000 | 100 | 0.050 | 218 | 92.14 |
| C2 | 2000 | 200 | 0.100 | 213 | 85.96 |
| C3 | 2000 | 300 | 0.150 | 175 | 69.44 |
| D1 | 1600 | 200 | 0.125 | 201 | 81.67 |
| D2 | 1800 | 200 | 0.111 | 187 | 81.45 |
| D3 | 2000 | 200 | 0.100 | 173 | 69.81 |

From the results obtained, it was found that the maximum shear strength was observed at rotational speed of 2000 rpm and traverse speed of 100 mm/min and the minimum was observed at rotational speed of 1600 rpm

and traverse speed of 300 mm/min. Both the maximum and the minimum shear strengths were observed when the TiC reinforcement particles were added but at different rotational and traverse speeds, respectively. It can be concluded from the results that the relationship between the fracture load and the traverse speed is inversely proportional. Increase in the traverse speed causes the fracture load to decrease. Shorter reaction time and lower reaction temperature is associated with higher traverse speed and this led to a decrease in the stirring period and the vertical movement of the material with the reinforcement, thereby affecting the strength of the bonding at the interface. It is obvious that the fracture load increases with an increase in the rotational speed for all the samples with reinforcement. As the rotational speed increased from 1600 rpm to 2000 rpm, substantial increase in the fracture load was observed. Higher rotational speed generated higher heat input because of higher friction heating which resulted in more intense stirring and mixing of the material.

It should be noted that the fracture load behaviour that occurred in the samples without reinforcement is reciprocal of results obtained with samples with reinforcement. The absence of the ceramic particle along the path of the weld seam exposed the weld interface to higher degree of thermal reaction, thereby making it to be very sensitive to temperature changes. As the rotational speed increases, the temperature around the weld zone increases, causing high turbulent mixture and stirring of the materials. Since there is no intermediate particle to balance the temperature change, the strength of the bonding will be compromised. However, once a sufficient rotational speed is achieved, further increase is not beneficiary to the mechanical properties.

Figure 11 shows the effect of the reinforcement particle on the fracture load. As can be seen, the presence of the TiC reinforcement particles contributed an appreciable strength change to the fracture load at higher rotating speed of 2000 rpm and do not show a remarkable improvement to the fracture load at rotational speed of 1600 rpm and 1800 rpm respectively, instead, it had an inverse effect on the strength.

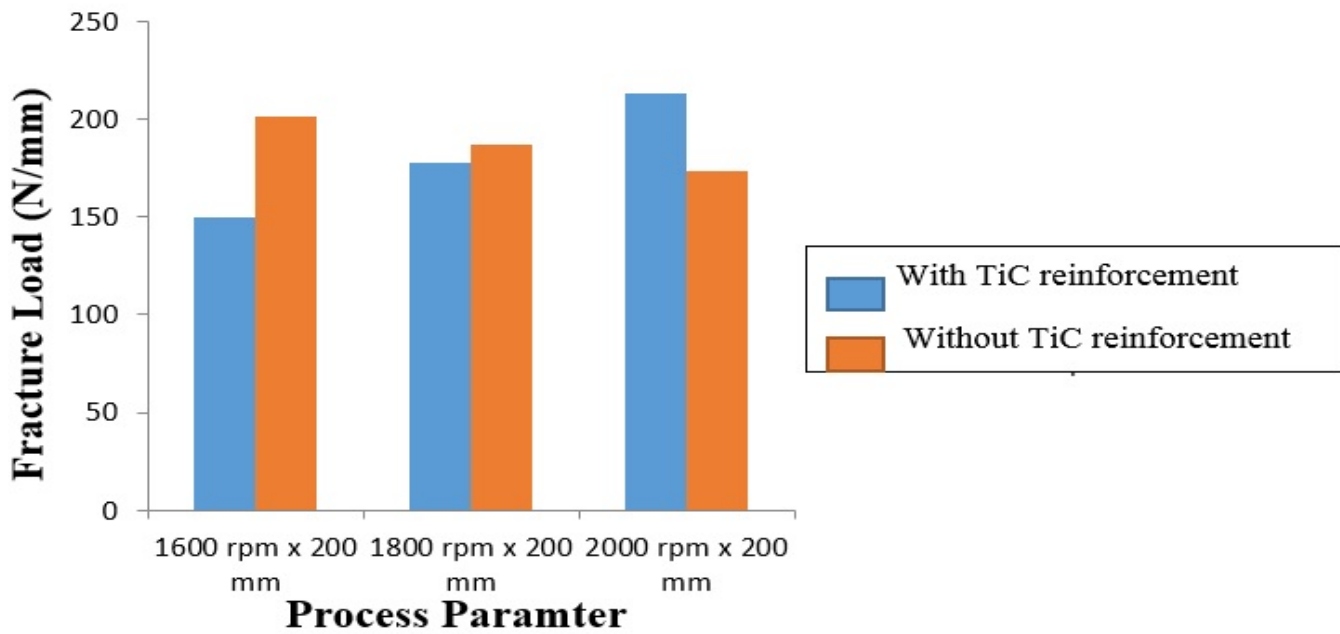


Figure 11 Fracture load against the process parameters

Slika 11 Fracture obremenitev proti procesnih parametrom

At rotational speed of 2000 rpm, the TiC homogenously mixed with the Al alloys properly, thereby forming a well-bonded matrix that yielded higher fracture strength. The presence of the ceramics particles constrained easy failure of material when under loading, thereby improved the mechanical strength of the matrix.

Joint efficiency

To estimate the joint efficiency of FS welds, the ratio of the tensile strength of lap shear specimens were compared to the tensile strength of the base metals. According to studies ²³, the tensile strength of lap shear specimen is derived from the fracture load per unit width to the effective sheet thickness (EST).

$$\text{Tensile strength of lap shear specimen} = \frac{\text{Fracture load per unit width}}{EST} \quad (1)$$

The EST is defined as the minimum sheet thickness determined by measuring the smallest distance between any un-bonded interface and the top surface of the upper sheet or the bottom surface of the lower sheet and it varies with the process parameter depending on the degree of bonding that exists between the weld interfaces. These phenomena should have apparent influences on the bearing-load of FSW lap-welded joints. Also presented in

Table 3 is the joint efficiency of the FSWed samples at different process parameters. From the result, the joint efficiency ranges from 52% to 92%. The highest was found at rotational speed of 2000 rpm and traverse speed of 100 mm/min.

The effect of the traverse speed on the EST was studied. Figure 12 shows the graphical relationship between the EST versus traverse speed. Traverse speed exhibits a linear relationship with the EST. As the traverse speed increased, the dimension of the EST also increased, thereby reducing the area of metallurgical bond that exists at the processed interface. Since the strength of the weld interface depends on the area of the metallurgical bond during the welding process, it is apparent that the relationship between the EST and the overall strength of the processed zone is exponential.

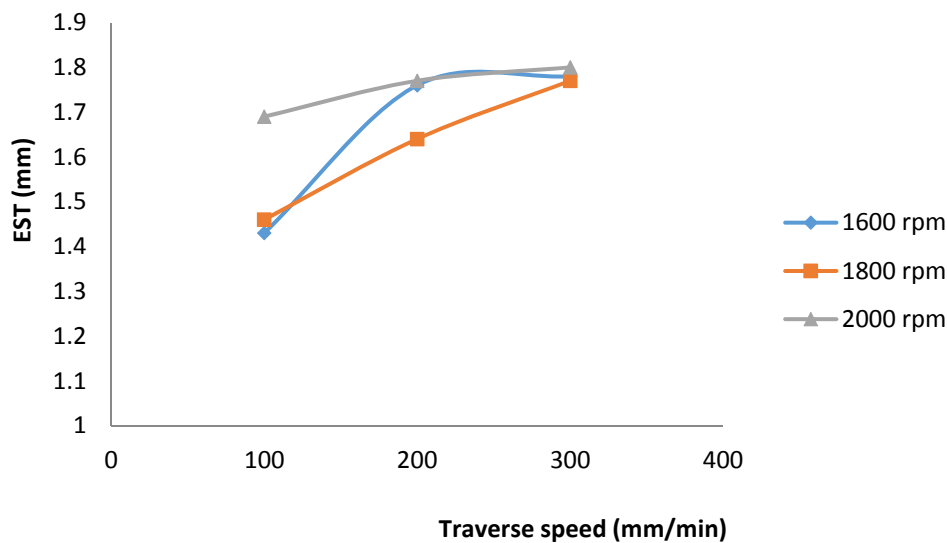


Figure 12 EST against the traverse speed

Slika 12 EST proti prečni hitrosti

Fracture behaviour

Four different modes of failure were noticed at the joint interfaces as illustrated in Figure 13. They are namely fracture mode (FM) 1, shear fracture that occurred due to lack of joint formation along the original interface of the two sheets. This led to pseudo metallurgical bond between the two sheets and the bond shear under tensile loading. Fracture mode 2 occurred on the advancing side hooking in which the crack initiates from the tip of the hook on the AS, propagates upward along the SZ/TMAZ interface and finally, the fracture at the SZ. Fracture mode 3 was noticed on the retreating side softening initiated from the hook and then linked to pores on the bottom plates caused by the diffusion of the bottom plate with the backing plate. The crack follows the sharp end of the groove to the other end. Fracture mode 4 failure took place close the base metal but the weld actually failed at the

HAZ on the advancing side of the weld. Table 4 lists the failure modes observed for each process parameter combination.

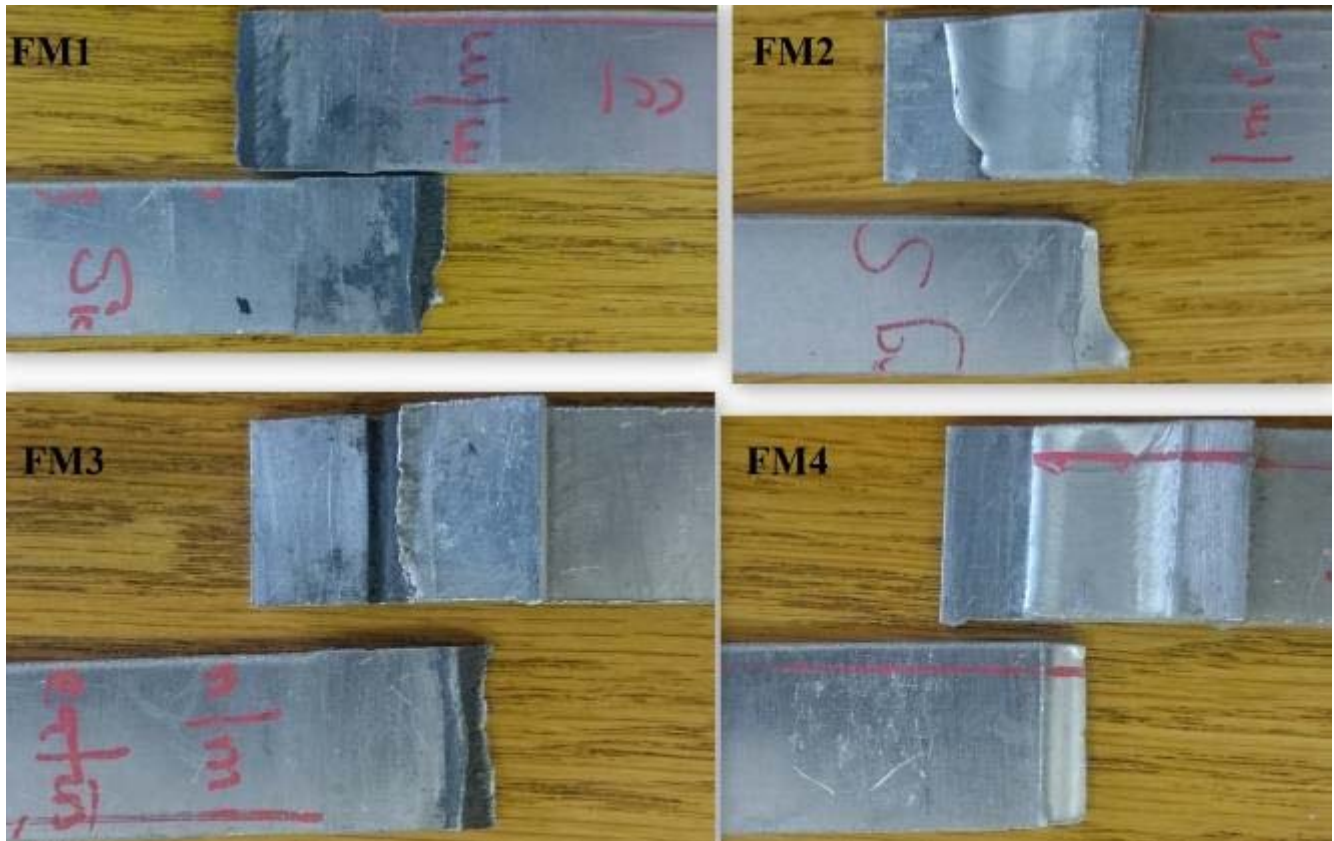


Figure 13 Fracture mode of the welded samples at different process parameters

Slika 13 Način Fracture varjenih vzorcih pri različnih procesnih parametrov

FM 1 was found at low rotational speed of 1600 rpm and high traverse speed of 300 mm/min. The dominant fracture modes are FM 3 and FM 4.

Table 4 Mode of fracture at different process parameters

Tabela 4 Način zloma na različnih procesnih parametrov

| Weld number | Rotational speed (rpm) | Traverse speed (mm/min) | Fracture Mode |
|-------------|------------------------|-------------------------|---------------|
| A1 | 1600 | 100 | FM 1/FM 2 |
| A2 | 1600 | 200 | FM 2 |

| | | | |
|----|------|-----|-----------|
| A3 | 1600 | 300 | FM 1 |
| B1 | 1800 | 100 | FM 3 |
| B2 | 1800 | 200 | FM 3 |
| B3 | 1800 | 300 | FM 4 |
| C1 | 2000 | 100 | FM 3/FM 4 |
| C2 | 2000 | 200 | FM 3 |
| C3 | 2000 | 300 | FM 4 |
| D1 | 1600 | 200 | FM 3 |
| D2 | 1800 | 200 | FM 4 |
| D3 | 2000 | 200 | FM 4 |

FM 1 is observed at low rotational speed and high traverse speed. This process condition is associated with low heat input that resulted in insufficient deformation and flow of the material forming pseudo weld. The crack initiation occurs through the gap tip of the unwelded area and went through the stir zone making the weld to shear into two at the welded area. This usually occurs when insufficient metallurgical bond is formed between the sheets.

FM 2 and FM 3 are the most dominating failure modes. The fracture mode is similar to normal tensile behaviour of aluminium alloy. The material went through necking for a period before eventually fracturing at the weakest zone.

The SEM images of the fracture surfaces were taken to determine the mode of fracture. Figure 14 illustrates the typical fractography features of surface failure.

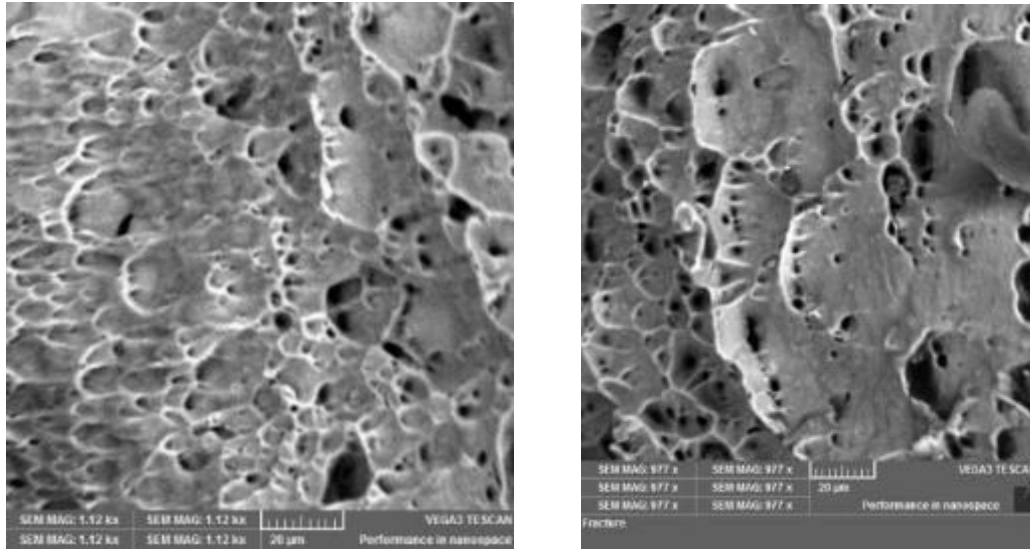


Figure 14 SEM images of the fracture surface at the fracture point for weld produced at rotational speed of 2000 rpm and traverse speed of 100 mm/min

Slika 14 SEM podoba preloma na točki preloma za vara pri vrtilni hitrosti 2000 obratov na minuto in prečni hitrosti 100 mm / min

The morphology of the failure mode shows large amount of fine dimples which confirm the amount of plastic flow prior to failure under tensile loading. The fine dimple feature observed indicate that the behaviour of fracture is ductile which implies that the lap joints exhibited ductile fracture during the lap shear tests.

4 CONCLUSION

Based on the observation from the results, the followings conclusions can be drawn

- The microstructural evolution correlates to the process parameters employed to produce welds. It was found that as the traverse speed increases, the evolving microstructure changed from elliptical to basin like shape at the interface.
- The microstructure revealed that the majority of the TiC particles were transported from the weld interface and deposited in the bottom sheet.
- The highest tensile value of 218 N/mm and joint efficiency of 92% was recorded for a weld produced at a high rotational speed of 2000 rpm and low traverse speed of 100 mm/min. This parameter combination setting can be recommended.

- The maximum hardness occurred at the stir zone and the minimum at the HAZ. The advancing side exhibited higher hardness distribution compared to the retreating side of the welds.

Acknowledgements

The authors would like to acknowledge the University of Johannesburg under the GES award scholarship of Postgraduate Research Centre for their financial support and the eNtsa Research Group of Nelson Mandela Metropolitan University (NMMU), Port Elizabeth, South Africa for allowing us to use their facility to produce the welds.

5 REFERENCES

1. Mishra RS, Ma Z. Friction stir welding and processing. *Materials Science and Engineering: R: Reports* 2005;50(1):1-78.
2. Kainer KU. *Metal matrix composites: Custom-made materials for automotive and aerospace engineering*. John Wiley & Sons; 2006. .
3. Fabrication of near-net shape graphite/magnesium composites for large mirrors. Orlando'90, 16-20 april International Society for Optics and Photonics; 1990. .
4. Miracle D. Metal matrix composites—from science to technological significance. *Composites Sci Technol* 2005;65(15):2526-40.
5. Rawal SP. Metal-matrix composites for space applications. *JOM* 2001;53(4):14-7.
6. Santo L, Paulo Davim J. *Surface engineering techniques and applications: Research advancements*. 2014:1-347.
7. P.O. Babalola, C.O. Bolu, A.O. Inegbenebor and K.M. Odunfa. Development of aluminium matrix composite, *International Journal of Engineering and Technology Research*. [revised 2014;2(1):1-11. .
8. Thomas WM, Nicholas ED, Needham JC, Murch MG, Temple Smith P, Dawes CJ, inventors. Friction stir welding. UK Patent Office, London patent . December 6, 1991.
9. Klobcar D, Kosec L, Pietras A, Smolej A. Friction-stir welding of aluminium alloy 5083. *Materiali in Tehnologije* 2012;46(5):483-8.

10. Gnetenjem IAZ. AA413. 0 and AA1050 joined with friction stir welding. *Materiali in Tehnologije* 2013;47(2):195-8.
11. Palanivel R, Mathews PK. The tensile behaviour of friction stir welded dissimilar aluminium alloys. *Materiali in Tehnologije* 2011;45(6):623-6.
12. Akinlabi ET. Characterisation of Dissimilar Friction Stir Welds between 5754 Aluminium Alloy and C11000 Copper 2011.
13. Sanders DG. Development of friction stir welding combined with superplastic forming processes for the fabrication of titanium structures. United States -- Washington: University of Washington; 2008:Source type: dissertations&theses; Object type: Dissertation; Object type: Thesis; Copyright: Copyright ProQuest, UMI Dissertations Publishing 2008; DOCID: 1555426411; PCID: 39316081; PMID: 66569; DocISBN: 9780549677864; DissertationNum: 3318447; PublisherXID: 3318447.
14. A. Elrefaey, M. Gouda, M. Takahashi, and K. Ikeuchi. Characterization of aluminum/steel lap joint by friction stir welding . March 2004.
15. Sharma V, Prakash U, Kumar BM. Surface composites by friction stir processing: A review. *J Mater Process Technol* 2015.
16. Akinlabi ET, Mahamood R, Akinlabi S, Ogunmuyiwa E. Processing parameters influence on wear resistance behaviour of friction stir processed al-TiC composites. *Advances in Materials Science and Engineering* 2014;2014.
17. Thangarasu A, Murugan N, Dinaharan I, Vijay S. Microstructure and microhardness of AA1050/TiC surface composite fabricated using friction stir processing. *Sadhana* 2012;37(5):579-86.
18. Jerome S, Bhalchandra SG, Babu SK, Ravisankar B. Influence of microstructure and experimental parameters on mechanical and wear properties of al-TiC surface composite by FSP route. *Journal of Minerals and Materials Characterization and Engineering* 2012;11(05):493.
19. Standard A. E3, standard guide for preparation of metallographic specimens. West Conshohocken, PA: ASTM International 2001.
20. STANDARD A. E92-82 E3. 1997: Standard test method for vickers hardness of metallic materials. Annual Book of ASTM Standards, ASTM.
21. Standard A. D1002-01, 2001, " Standard Test Method for Apparent Shear Strength of Single-Lap-Joint Adhesively Bonded Metal Specimens by Tension Loading (Metal-to-Metal)." ASTM International, West Conshohocken, PA, 2001, DOI: 10.1520/D1002-10.
22. Standard A. E8/E8M-13a, standard test method for determining volume fraction by systematic manual point count. Aug., ASTM International, West Conshohocken, PA 2013.
23. Xu X, Yang X, Zhou G, Tong J. Microstructures and fatigue properties of friction stir lap welds in aluminum alloy AA6061-T6. *Mater Des* 2012;35:175-83.

